Applied Catalysis B: Environmental 129 (2013) 30–38

Contents lists available at SciVerse ScienceDirect

Applied Catalysis B: Environmental

journal homepage: www.elsevier.com/locate/apcatb

Promoting effect of calcium doping on the performances of MnO_x/TiO_2 catalysts for NO reduction with NH_3 at low temperature

Tingting Gu[a,c], Ruiben Jin[b,c], Yue Liu[a,c,*], Hongfeng Liu[a,c], Xiaole Weng[a,c], Zhongbiao Wu[a,c,*]

[a] Department of Environmental Engineering, Zhejiang University, Hangzhou 310058, PR China
[b] Environmental Science & Design Research Institute of Zhejiang Province, Hangzhou 310058, PR China
[c] Zhejiang Provincial Engineering Research Center of Industrial Boiler & Furnace Flue-gas Pollution Control, Hangzhou 310058, PR China

ARTICLE INFO

Article history:
Received 13 March 2012
Received in revised form 14 August 2012
Accepted 2 September 2012
Available online 13 September 2012

Keywords:
NH_3-SCR
Low temperature
Ca doping
MnO_x/TiO_2

ABSTRACT

In this paper, the Ca doped MnO_x/TiO_2 catalysts were synthesized through a sol–gel method, which exhibited promoting effects on selective catalytic reduction (SCR) of NO with NH_3 at low temperature. The NO conversion of MnO_x/TiO_2 had been greatly improved from ca. 40% to 90% at 140 °C after Ca doping. After the catalysts being subjected to a variety of analytical measurements, we observed that the addition of Ca could result in better dispersion of MnO_x on TiO_2, leading to the enhancement of BET surface area and pore volume. This could be attributed to the strong interactions among calcium, manganese oxides and titania. Furthermore, an obvious increase in the amounts of ad-NO_x species, especially monodentate nitrate and NO_2^- species, was also observed. All of these would give the contributions to the great improvement of catalytic activity by the addition of Ca.

1. Introduction

Selective catalytic reduction (SCR) of NO_x by NH_3 has been extensively used to treat stationary exhausts [1,2]. The commercialized industrial catalysts for NH_3-SCR of NO are WO_3-V_2O_5/TiO_2 and MoO_3-V_2O_5/TiO_2, whose operation temperature windows are normally at 300–400 °C. As such, their catalyst beds have to be located upstream of the desulfurizer and the particulate control device to avoid reheating of the flue gas. This makes these catalysts susceptible to deactivation from high-sulfur and high-dust. Furthermore, retrofitting SCR devices into existing systems is costly because the space and access in many power plants are extremely limited. Therefore, it is a great interest to develop active low-temperature SCR catalysts that could be placed downstream of the flue gas.

Widespread attentions have been paid to the development of low-temperature SCR catalysts in recent years. In particular, manganese oxides (MnO_x) were studied the most extensively because of their various types of labile oxygen in crystalline lattice, which are beneficial to low-temperature SCR reaction [3]. For example, the manganese based catalysts, such as pure manganese oxides [4] and MnO_x supported on Al_2O_3 [5], TiO_2 [6,7], zeolite [8,9], CeO_2 [10,11], and active carbon [12] had all exhibited favorable activity in the low-temperature SCR process.

The modification of low-temperature Mn-based SCR catalysts has been also extensively investigated for better performance, such as transition metal doping [13], ceria doping [14], etc. Very recently, Ca modification of $MnCr_2O_4$ catalyst was proposed by Zamudio et al. [15] for low-temperature SCR reaction. And an enhanced NO conversion of 96% at 125 °C was obtained after Ca doping. It was reported that Ca doping could improve the mobility of oxygen [16], electron donation capacity [17] and dispersion of active phase [18], resulting in the enhancement of catalytic activity. Therefore, the authors were motivated to make calcium modifications of MnO_x/TiO_2 catalysts based on our previous work for low-temperature SCR reaction.

However, for NH_3-SCR system, Ca deposition was normally known as its poisoning effect on the catalytic activity due to the decrease in the amount and stability of Brönsted acid sites [19,20]. In our previous study [21], the surface deposition of CaO would also do harm to the low-temperature SCR performance because of less amount of acid sites after Ca doping. To reduce this effect, more Ca atom needed to enter into the crystal lattices of the catalysts. Accordingly, sol–gel route was utilized to achieve highly dispersed Ca modified MnO_x/TiO_2 catalysts in this paper. A rang of analytical techniques, including BET, XRD, TEM, XPS, TPR, TPD, DRIFT, etc., were used herein to evaluate the effects of Ca doping on their low-temperature SCR reaction behaviors.

* Corresponding authors at: Department of Environmental Engineering, Zijingang Campus, Zhejiang University, Yuhangtang Road 388, Hangzhou 310058, PR China. Tel.: +86 571 87953088; fax: +86 571 87953088.
E-mail addresses: yueliu@zju.edu.cn (Y. Liu), zbwu@zju.edu.cn (Z. Wu).

0926-3373/$ – see front matter © 2012 Elsevier B.V. All rights reserved.
http://dx.doi.org/10.1016/j.apcatb.2012.09.003

2. Experimental methods

2.1. Catalysts preparation

Tetrabutyl titanate (0.1 mol), manganese nitrate (0.04 mol), ethanol (0.8 mol), water (0.6 mol) and acetic acid (0.3 mol) were mixed under vigorous stirring at room temperature to form transparent sol. The molar ratio of precursor used above was the optimal value obtained in our previous study for MnO_x/TiO_2 [7]. Calcium amount (0–5 wt.%) of calcium nitrate was added during this process for different catalysts. The sols transformed to gels after stabilized at room temperature for two weeks. The gels were dried at 110 °C to remove organic solution. Then the solids were calcined at 500 °C in air for 6 h in a tubular furnace and then crushed and sieved to 40–60 meshes. The catalysts were denoted as Ca(x) MnTi in this paper, where x represented the weight ratio of CaO to MnO_x/TiO_2.

2.2. Catalytic activity tests

SCR activity measurements were carried out in a fixed-bed quartz tubular flow reactor (i.d. 9 mm) at low temperature window (60–200 °C) containing 2 g catalyst (1.5 ml volume) with a gas hourly space velocity (GHSV) of 75,000 h^{-1}. The reactant gas typically consisted of 650 ppm NO, 650 ppm NH_3, 3% O_2 and balance N_2. The concentrations of NO, NO_2 and O_2 were monitored by non-dispersive infrared (NDIR)-based gas analyzer (Photon-PGD-100 Madur Electronics).

2.3. Catalysts characterization

The textural structures were measured by N_2 adsorption at 77 K in a Micromeritics ASAP 2020 system, and specific surface areas of samples were measured using Brunauer–Emmett–Teller (BET) method. The pore size distributions were measured from the N_2 desorption isotherm using the cylindrical pore model (BJH method). The morphology, structure, and grain size of the samples were examined by transmission electron microscopy (TEM: JEM-2010).

X-ray diffraction patterns (XRD) of the samples were recorded on a Rigaku D/Max-RA powder diffractometer using Cu Kα radiation (40 kV and 150 mA). X-ray photoelectron spectroscopy (XPS) was used to analyze the surface atomic state of catalyst with Al Kα X-rays (Thermal, ESCALAB 250). The shift of the binding energy due to relative surface charging was corrected using the C 1s level at 284.8 eV as an internal standard. The concentrations of Ca, Mn, Ti and O on catalysts surface were calculated from the peak areas ratios of the samples.

Temperature programmed reduction (TPR) and Temperature programmed desorption (TPD) were carried out on a custom-made TCD setup using 50 mg samples. Prior to TPR and TPD experiments, samples were pretreated in pure He at 400 °C for 1 h. TPR runs were carried out with the linear heating rate (5 °C/min) in pure N_2 containing 6% H_2 at a flow rate of 30 ml/min. For NH_3-TPD or NO-TPD experiments, after the pretreatment, catalysts were saturated with anhydrous NH_3 (4% in He) or NO (4% in He) at a flow rate of 30 ml/min for about 30 min. Desorption was carried out by heating these samples in He (30 ml/min) from 100 to 430 °C with a heating rate of 5 °C/min.

FT-IR spectra were acquired using an in situ DRIFT cell equipped with a gas flow system. The DRIFT measurements were performed with ZnSe windows coupled to Nicolet 6700 FTIR spectrometers. In the DRIFT cell, the catalyst was pretreated at 400 °C in a He environment for 2 h, and then cooled to 150 °C. The background spectrum was recorded with flowing He and was subtracted from the sample spectrum.

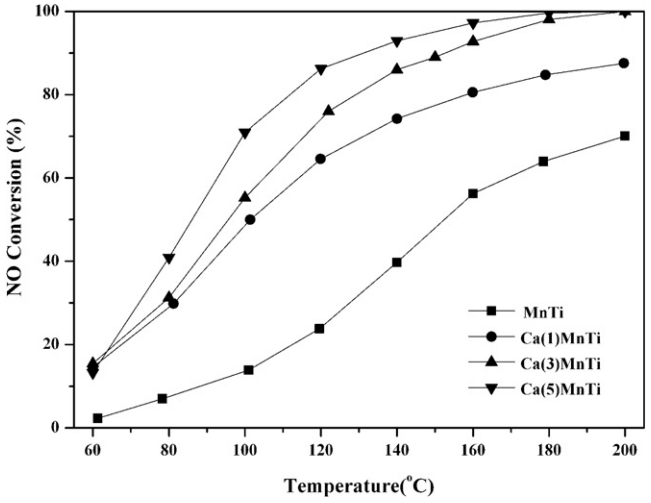

Fig. 1. NO conversion over CaMnTi catalysts. Reaction conditions: 650 ppm NO, 650 ppm NH_3, 3% O_2, and balance N_2, GHSV = 75,000 h^{-1}.

3. Results and discussion

3.1. Catalytic activity tests

Fig. 1 depicted the NO conversion within the temperature range of 60–200 °C over MnTi catalysts modified with various Ca loadings. As expected, at a relatively high gas hourly space velocity (GHSV) of 75,000 h^{-1}, the activity of MnTi sample did not show a good performance, revealing only about 40% NO conversion at 140 °C. However, with the increase in Ca loading, the catalytic activity was significantly promoted, where more than 90% NO conversion efficiency was achieved at 140 °C for Ca(5) MnTi sample. And the further increase in Ca content would make the gels unstable in the preparation procedure, so that the SCR activity was quickly decreased. Moreover, the N_2O productivity was obviously inhibited by Ca doping (see Fig. S1). The effect of H_2O (3.5%) on catalytic performance of Ca doped catalysts was also investigated (see Table S1). It could be clearly seen that the H_2O would have a strong negative effect on NO conversion at low temperature, while the N_2O formation amount was also inhabited in the presence of H_2O. Furthermore, it was found that this inhibition effect was strengthened as the increasing of Ca loading content. For instance, the NO conversion was decreased by about 40% for Ca(5) MnTi at 100 °C, while that was around 23% for Ca(1)MnTi. This may be attributed to the stronger affinity of calcium oxide to H_2O.

3.2. XRD analysis

Fig. 2 illustrated the XRD patterns of the CaMnTi catalysts with different Ca loadings. From the XRD results, it could be seen that for the MnTi sample, TiO_2 existed as a mixing form of anatase and rutile, where the anatase dominated the phases. There were no peaks corresponding to manganese oxides in the sample, implying that the manganese oxides were well dispersed. Furthermore, the intensities of XRD peaks due to TiO_2 rutile phase were declined with the increase of Ca loading. As for Ca(5) MnTi sample, TiO_2 exhibited almost anatase phase with the rutile phase rarely absent. Similar results could be found in the literature [22] that Ca doping could produce more stable antase phase prepared by sol–gel method. They argued that the alkaline earth metal with large ionic radii of cations would elevate the anatase–rutile transition temperature of the titania, thereby inhibit the formation of rutile phase. This result revealed that the doped Ca could suppress the formation of rutile phase, which was favorable for SCR activity as it was reported that

Table 1
Physical property of catalysts at different Ca contents.

Catalysts	BET surface area (m^2/g)	Pore volume ($\times 10^{-2}$ cm^3/g)	Average pore diameter (nm)
MnTi	53.5	16.79	9.32
Ca(1) MnTi	59.3	18.85	8.64
Ca(3) MnTi	87.9	21.63	7.08
Ca(5) MnTi	98.7	22.14	6.49

the anatase phase was more active than rutile phase for SCR catalysts [23–25]. Moreover, for Ca(1) MnTi sample, a mixed oxide of Mn and Ca ($Ca_{0.9}Mn_{0.1}O$) was detected, which had two main peaks at 32.4° and 37.6° (PDF# 36-1378) and the latter one might be overlapped by the strong peak at 37.8° assigned to anatase phase. And this band became weaker with further increase of Ca content. In all, the increase of Ca doping content would lead to the decrease of the crystallinity of the samples owing to the strong interactions among calcium, MnO_x and titania.

3.3. Morphology and structure investigation

We have selected MnTi and Ca(5) MnTi (with best activity) samples for further investigation by TEM and HRTEM (as shown in Fig. 3). It can be seen that the particle size of Ca(5) MnTi sample was slightly smaller than that of MnTi sample, indicating that the Ca doping could somewhat decrease the particle sizes of the catalyst. As illustrated in Fig. 3b and d, clear lattice fringes could be observed for both MnTi and Ca(5) MnTi samples. The lattice plane distance of TiO_2 was calculated to be 0.352 nm, matched with the [1 0 1] plane of anatase phase (PDF# 21-1272). Another lattice fringes with lattice plane distances at about 0.243 nm and 0.192 nm observed in Fig. 3c and 3d were corresponded to [2 1 1] and [3 1 1] orientations of MnO_2 (PDF# 44-0142), respectively. In Fig. 3c and 3d, the average particle size of MnO_2 for MnTi sample was approximately 14 nm, while for Ca(5) MnTi sample was about 10 nm, revealing that the loading of Ca was beneficial to manganese oxide dispersion, which further confirmed the XRD results. This could lead to the strong interaction of Ca with MnO_x and TiO_2, inhibiting the sintering of samples.

3.4. BET-BJH analysis

Table 1 showed structure and textural data along with the increase of Ca loading. As shown in the Table, the BET surface areas and pore volumes sharply increased with increasing the loading of Ca. Particularly, when the Ca loading increased from 1 wt.% to 3 wt.%, the BET surface area was significantly shifted from 59.3 to 87.9 m^2/g. The pore size distributions determined by BJH method (see Fig. 4) also showed similar trend. These variations might be attributed to smaller particle size and better dispersion of the catalysts after Ca doping (see Fig. 3), where the reduction in particle size would increase the exposed area of the catalysts, leading to the elevation of surface area and better dispersion of the catalysts would keep more space between the particles and avoid the collapse of microspores.

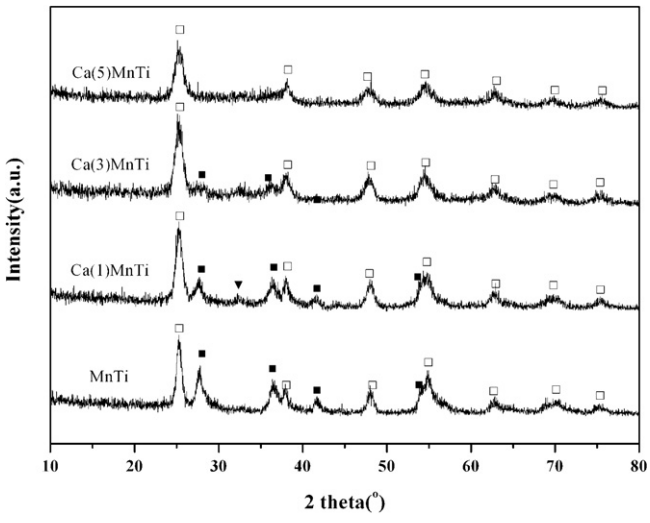

Fig. 2. XRD profiles of CaMnTi catalysts with different Ca contents (□ – anatase TiO_2, ■ – rutile TiO_2, ▼ – calcium oxide).

3.5. Temperature programmed desorption (TPD) measurements

The NH_3-TPD profiles of CaMnTi samples with various Ca loadings in the range of 100–430 °C were revealed in Fig. 5. It could be seen that desorption of ammonia occurred over a wide temperature range, due to the presence of adsorbed ammonia species with different thermal stability. All curves exhibited two peaks. The desorption peaks at around 170 °C (noted as α) were assigned to weakly adsorbed ammonia, which were mainly due to the physical adsorbed ammonia. And the desorption peaks at about 280 °C (noted as β) would be probably assigned to the chemical adsorbed ammonia at Lewis and Brönsted acidity sites. The adsorption amounts of ammonia were further calculated and the results were listed in Table 2. It could be obtained that the total NH_3 adsorption capacity was increased by Ca doping and the specific NH_3 adsorption capacity was first slightly increased and then obviously decreased. Although the adsorbed amount for each peak did not be calculated, it could be clearly seen in Fig. 5 that the first desorption peak assigned to physical adsorption of NH_3 increased quickly with the Ca doping content, since the BET surface area was enlarged greatly with the doping of Ca. However, the second peak due to the chemical adsorbed NH_3 did not increase so far because the basic component of Ca was added thereby lower the acidic strength of the catalysts [19]. Overall, this confirmed that the Ca doping would have somewhat negative effect on the acidity of the samples.

Fig. 6 depicted the TPD profiles of NO for the CaMnTi samples in the temperature of 100–430 °C. The MnTi sample showed single NO desorption peak centered at around 160 °C, assigned to the decomposition of weakly bound nitrite species (ad-NO_2^-) [15,26]. Ca doped samples showed different NO-TPD profiles, in which two distinct desorption peaks of NO were observed: one large peak was centered at about 160 °C and the other was centered at around 360 °C that was always due to the decomposition of strongly bound nitrate species (ad-NO_3^-) [15,26–28]. Furthermore, both the desorption peaks grew up with the increase of Ca loading. The adsorption amounts were also calculated (Table 2) and it could be found that the specific NO adsorbed amount increased with the Ca doping content although the surface area was dramatically increased. This further confirmed that the basicity of the catalyst after Ca doping was greatly improved. These results were also in accord with the results reported by the Yang et al. [18] that Ca doping could increase the NO adsorbed amount over the catalysts.

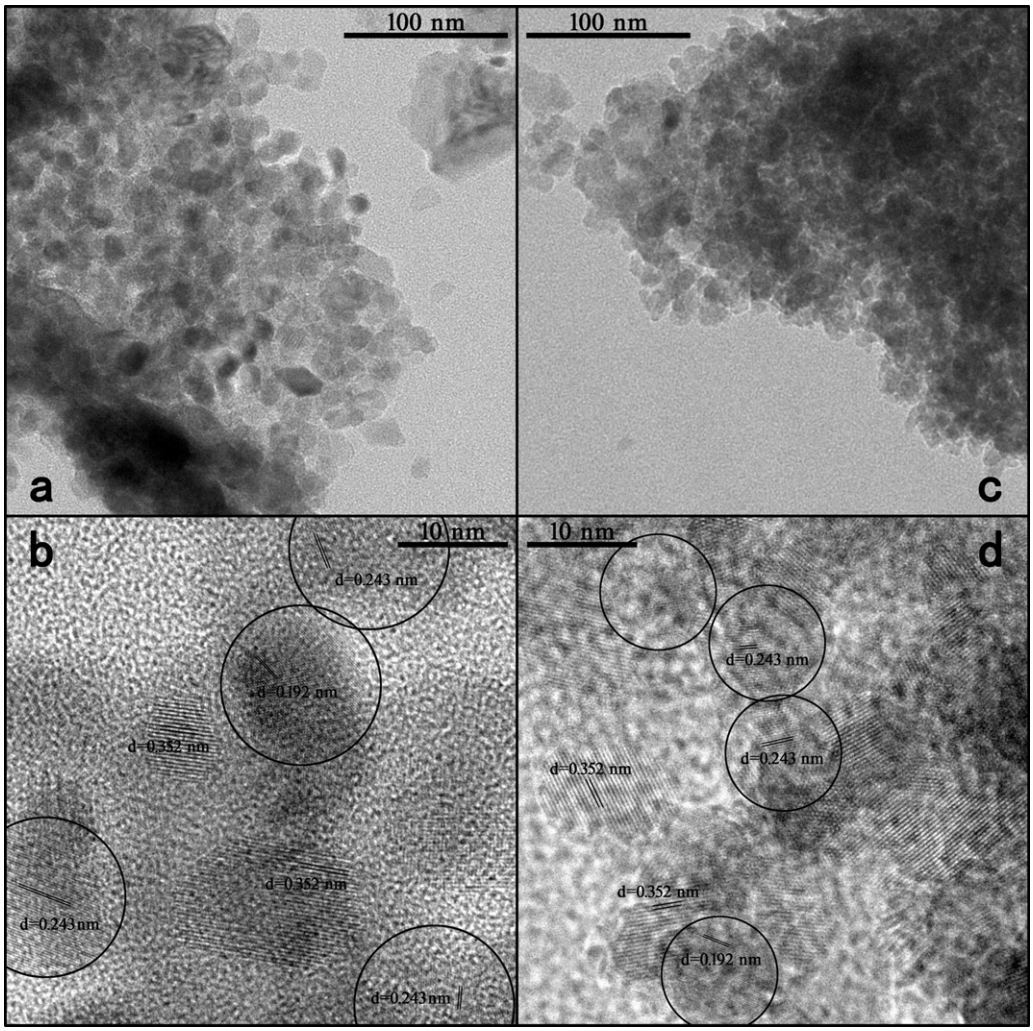

Fig. 3. TEM and HRTEM images of MnTi (a, b) and Ca(5)MnTi (c, d) samples.

3.6. Temperature programmed reduction (TPR) measurement

In order to investigate the effect of Ca doping on the reducibility of the catalysts, H_2-TPR profiles of CaMnTi catalysts with various Ca loadings were shown in Fig. 7. As displayed, there was one broad peak spanned within the temperature range of 200–500 °C for the MnTi sample, which was corresponded to the following successive reduction steps: MnO_2–Mn_2O_3–Mn_3O_4–MnO [4]. Broad peaks could also be observed for the CaMnTi samples and it was worthy of note that their reduction peaks of MnO_x slightly shifted to higher temperatures, together with the total amounts of hydrogen consumption within the temperature range of 200–500 °C decreased. A similar phenomenon was also observed by Pour et al. [29] over Fe/Cu/SiO_2 catalyst, where the authors attributed it to the improvement of catalysts basicity. Guerrero et al. [30] also found that alkali (sodium) addition would lead to an increase in the reduction temperature for Cu/TiO_2 catalysts. Another interesting fact was that a weak peak located firstly at 578 °C for MnTi sample became stronger and shifted to higher temperature (626 °C for Ca(5) MnTi) with an increase in Ca doping. It was reported that the reduction of MnO_x to Mn^{2+} was completed up to 550 °C [4] and further reduction to metallic Mn^0 did not proceed until 1200 °C [31]. Therefore, this peak might be ascribed to the reduction of Mn cations, which had strong interaction with TiO_2 (e.g., the reduction of Mn^{n+}–O_x–Ti [32,33]). These changes implied that the addition of Ca would strengthen the Mn–Ti interactions, which were more resistant to reduction. These results agreed well with the findings of the literature [18], in which Yang et al. found that the introduction of Ca would make the reduction $CuZrO_x$ more difficult, attributing to the changes to the interactions among Ca and the other metal oxides. Actually, the strong interactions between Ca dopants and MnO_x or TiO_2 would inhibit the sintering of MnO_x and titania during calcination process, thereby improved the surface area and the dispersion of active phase. These all enhanced the SCR activity. Similar results

Table 2
The total and specific NH_3 and NO adsorption amount for catalysts.

Catalysts	Total NH_3 adsorbed amount (mmol/g)	Specific NH_3 adsorption amount (mmol/m^2)	Total NO adsorbed amount (mmol)	Specific NO adsorption amount (mmol/m^2)
MnTi	3.49	0.065	1.49	0.028
Ca(1)MnTi	4.09	0.069	2.78	0.052
Ca(3)MnTi	4.87	0.055	4.25	0.080
Ca(5)MnTi	4.79	0.049	3.83	0.072

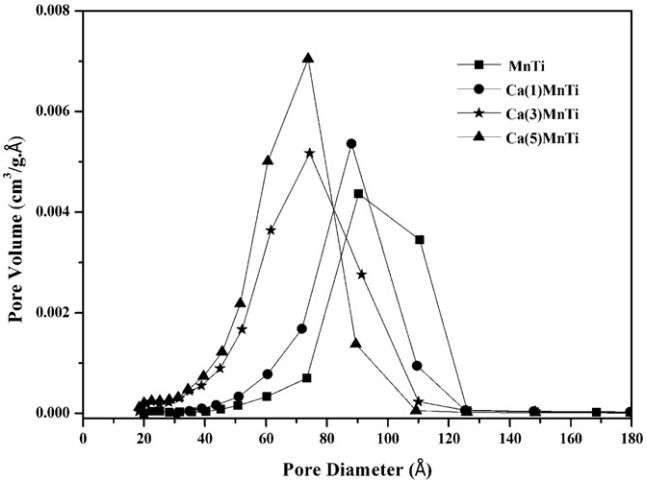

Fig. 4. BJH desorption pore size distributions.

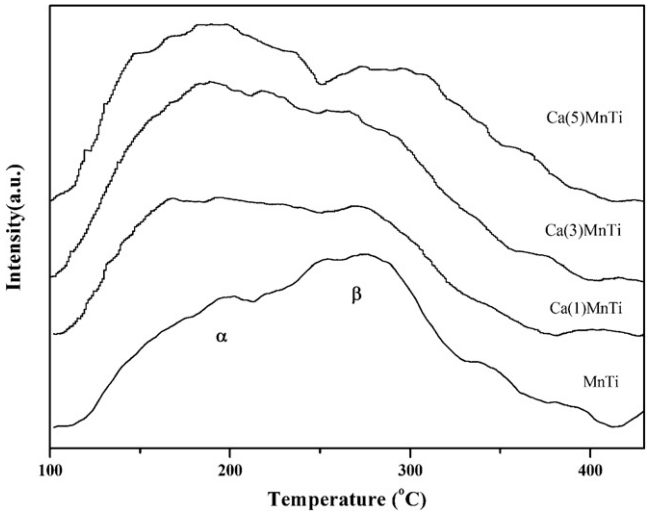

Fig. 5. NH_3-TPD profiles of CaMnTi catalyst with different Ca contents.

could be found in the literature [34] for transition metal doped MnO_x/TiO_2 catalysts. As for the increase in N_2 selectivity, according to Tang et al.'s work [35], it was indicated that the better reducibility of MnO_x catalysts, the easier production of N_2O during SCR process.

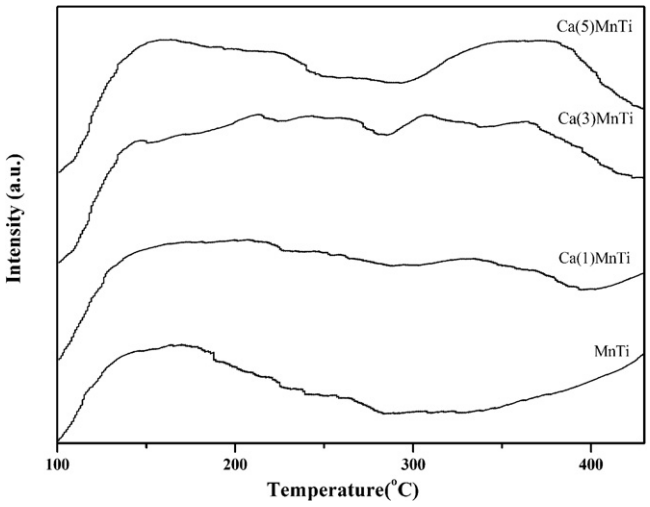

Fig. 6. NO-TPD profiles of CaMnTi catalyst with different Ca contents.

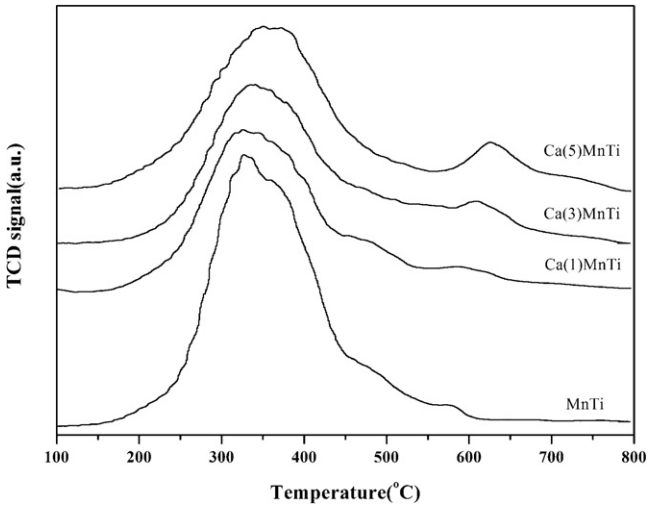

Fig. 7. H_2-TPR profiles for CaMnTi catalysts with different Ca contents.

The increasing N_2 selectivity was mainly attributable to the reason that Ca doping decreased the reducibility of the catalyst due to its more basic properties.

3.7. XPS analysis

The samples were further analyzed using XPS to identify the surface nature and the results were given in Fig. 8 and Table 3. Fig. 8(I) showed the binding energies of Ti 2p photoelectron peaks at 458.5 eV and 464.3 eV for Ti 2p3/2 and Ti 2p1/2 lines, respectively, corresponding to Ti (IV) in a tetragonal structure [36,37]. As shown, when Ca was introduced, the binding energy of the Ti 2p peaks slightly shifted to lower binding energy. It had been reported that Ti—O—Ti linkages of TiO6 octahedra were broken in strong alkali solution, leaving some oxygen vacancies in the formation of nanotubes [38–40]. Hence, it was conjectured that this shift in binding energy might be due to the vacancies created by O_2 because of Ti—O—Ti bonds breaking. The shift of binding energy of the Ti 2p peaks might be an indication of oxygen vacancies, which was induced by Ca loading. From the XPS results, we concluded that the local structure around the Ti ion in the Ca contained samples was different from the local structure around the Ti ion in MnTi.

The Mn 2p region consisted of a spin-orbit doublet with Mn 2p1/2 at a BE of about 653.3 eV and Mn 2p3/2 at about 642.0 eV, revealing the characteristic of a mixed-valence manganese system (Mn^{4+} and Mn^{3+}) [41] (see Fig. 8(II)). According to the references [6,42,43], as seen in Fig. 8(II), the Mn 2p3/2 spectra was split into two peaks at 642.9 eV and 641.6 eV, which were ascribed to Mn^{4+} and Mn^{3+}, respectively. With the increase of Ca doping, Mn 2p peaks spread to higher binging energy range, revealing the increase of higher oxidation state of Mn species. Furthermore, as shown in Fig. 8(III), the binding energy of Ca $2p_{2/3}$ was observed at 346.9 eV, which was slightly lower than the binding energies of bulk CaO at 347.2 eV [44]. Both of the changes indicated that there were strong interactions between Ca, Ti and Mn components, probably forming a new solid solution phase. This finding was in great agreement with the abovementioned analysis of XRD, TEM and H_2-TPR results.

As shown in Fig. 8(IV), the O1s spectrum could be deconvoluted into three constituents, corresponding to various oxygen containing chemical bonds. According to the literature [45–47], the first peak at 529.7 eV was assigned to lattice oxygen atoms (noted as O_a); the second one at 531.3 eV was attributed to surface-adsorbed oxygen (noted as O_b); the third oxygen peak at ca.532.1 eV was originated from chemisorbed water (noted as O_c). As listed in Table 3, with the increase of Ca doping, the chemisorbed oxygen O_b content

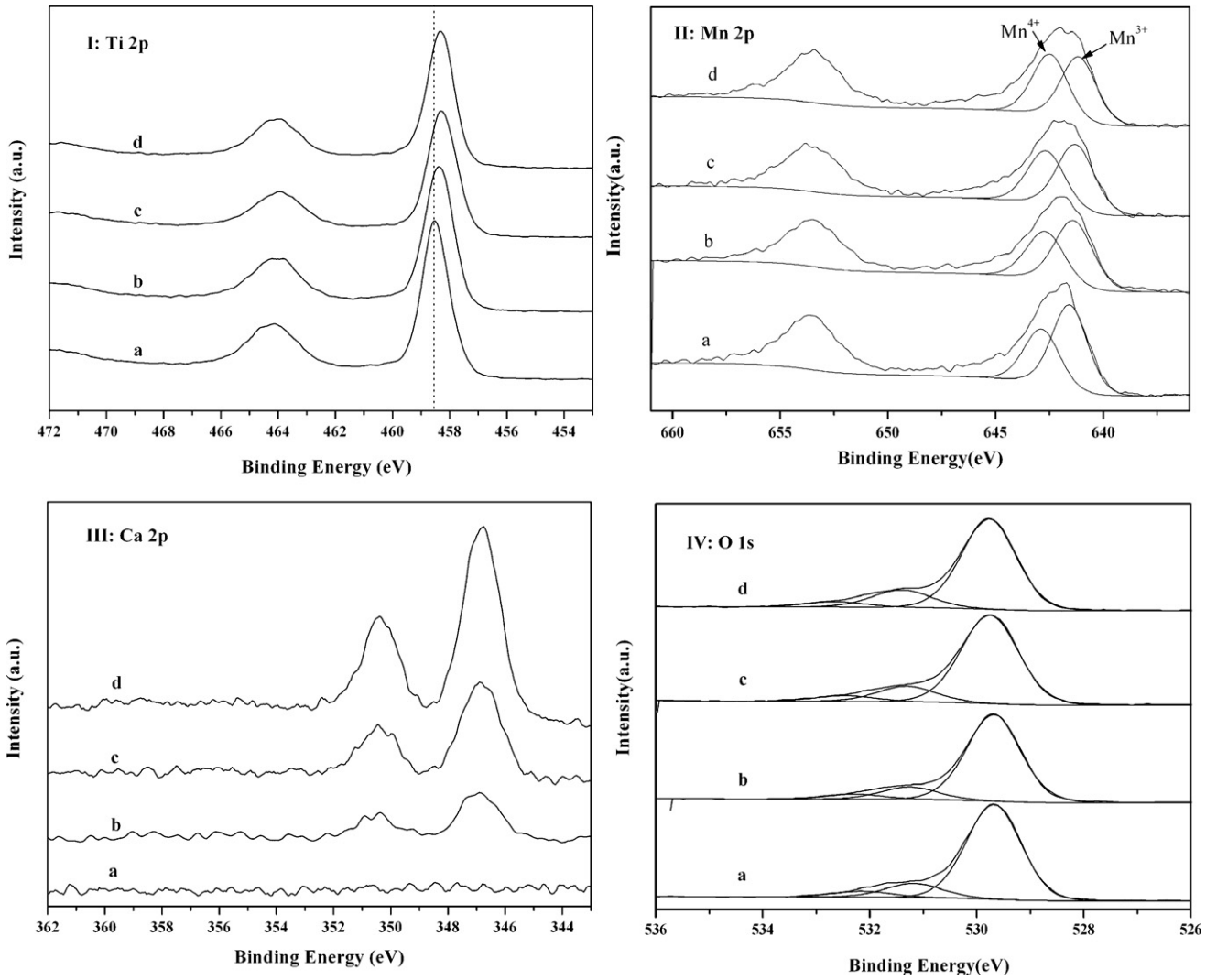

Fig. 8. XPS region of catalysts: (I) Ti 2p, (II) Mn 2p, (III) Ca 2p, (IV) O 1s (a: MnTi, b: Ca(1)MnTi, c: Ca(3)MnTi, d: Ca(5)MnTi).

was gradually increased. This is a promising result as the surface chemisorbed oxygen was the most active oxygen in SCR reaction [48]. The enhanced oxygen mobility after Ca doping was reported in the literature [16], which might support this finding.

3.8. DRIFT of NO and NH_3 adsorption

The adsorption of NO on MnTi catalyst at 150 °C was shown in Fig. 9A. The spectrum taken after 30 min of NO adsorption was characterized by the bands at 3522, 1907, 1843, 1610, 1585, 1533, 1495, 1443, 1282, 1248 and 1009 cm^{-1}. Further evacuation for 30 min had caused a disappearance of bands at 1907 and 1843 cm^{-1} and a decrease in the intensity of bands at 1610, 1495 and 1282 cm^{-1}. The bands at 1907 and 1843 cm^{-1} were attributed to the coordination of a NO molecule to a Lewis acid (metal sites) via nitrogen atom [49,50], which disappeared after He purging. According to the literatures [51–53], the bands in the region of 1600–1200 cm^{-1} were due to typical of NO_3^- species coordinated to the catalyst surface. As such, the absorption bands observed could be attributed to bridged (1603 cm^{-1}), bidentate (1585, 1533, 1248 cm^{-1}), monodentate (1495, 1282 cm^{-1}) nitrates. The band at 1624 cm^{-1} was assigned to the adsorbed NO_2 on oxide surfaces [54], at 1009 cm^{-1} attributed to the cis-$N_2O_2^{2-}$ species [55] and at 1443 cm^{-1} showed the formation of monodentate nitrite species [56]. A negative absorption at 3684 cm^{-1} was corresponded to isolated surface OH groups [49,57] whereas the broad positive band at 3522 cm^{-1} was attributed to H-bonded hydroxyls [49,57]. These observations could be attributed to the water producing as the formation of the NO_2 and nitrate species with the vicinity of the surface hydroxyls [50].

Table 3
Surface atomic concentration of catalysts with different Ca contents.

Catalysts	Surface atomic concentrations (%)						
	Mn	Ti	Ca	O_a	O_b	O_c	O_{total}
MnTi	12.29	18.82	0	56.47	8.69	3.73	68.89
Ca(1)MnTi	11.67	18.73	0.80	56.72	8.65	3.42	68.79
Ca(3)MnTi	10.92	18.42	1.31	56.00	9.81	3.53	69.35
Ca(5)MnTi	11.34	17.01	2.33	54.45	11.35	3.53	69.33

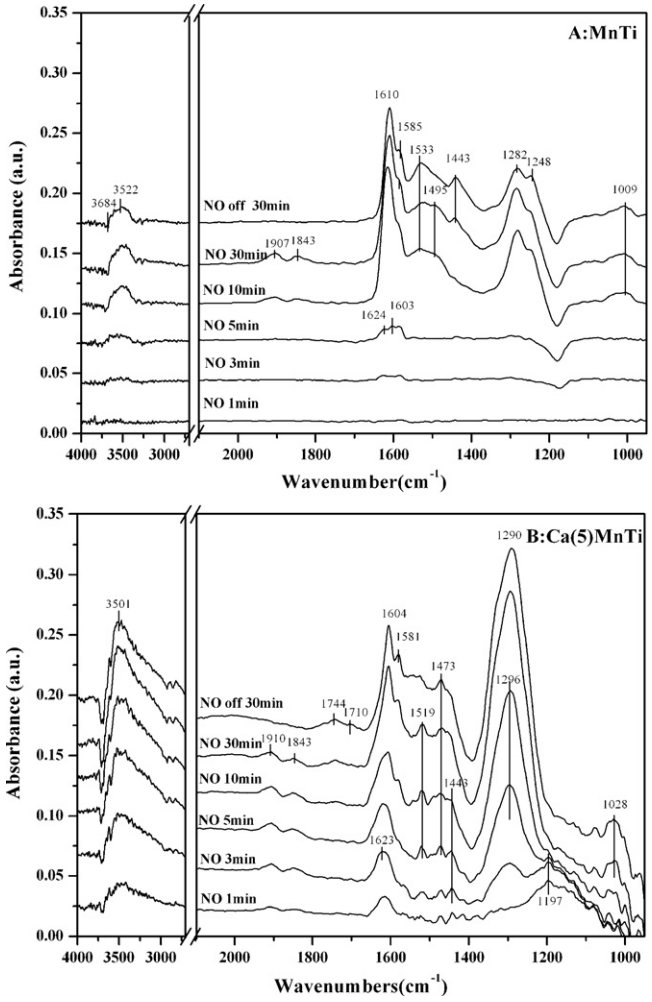

Fig. 9. DRIFT spectra taken at 150 °C upon passing 1000 ppm NO/He over (A) MnTi and (B) Ca(5) MnTi catalysts for different times and evacuation.

Compared with the NO adsorbed on the MnTi catalyst, the DRIFT spectra for NO adsorbed on Ca(5) MnTi catalyst at 150 °C as displayed in Fig. 9(B) was basically the same except the great increase in the intensity. However, there were still some differences. Firstly, there was a new weak band at 1744 cm^{-1} with a shoulder peak at 1703 cm^{-1} over Ca(5) MnTi catalyst, arising with the NO adsorption and remained after evacuation. Since the typical band of N_2O_4 is at 1748–1740 cm^{-1}, sometimes accompanied by a small shoulder around 1710 cm^{-1} [58], they could be assigned to N_2O_4 species due to NO_2 dimerization. Secondly, after introduction of NO, a wide band with a maximum at 1197 cm^{-1} immediately occurred and then vanished after 5 min. It was reported that anionic nitrosyl NO^- species had been observed when NO was adsorbed on alkaline earth metal oxides such as MgO [59] and CaO [60], giving rise to absorption in the 1195–1100 cm^{-1} region. Thus, the band lied at 1197 cm^{-1} was probably assigned to anionic nitrosyl NO^- species. And the band at 1443 cm^{-1} ascribed to NO_2^- species also appeared in the NO flowing on Ca(5) MnTi catalyst, which had higher intensity compared with that of MnTi catalyst. Otherwise, it was interesting that monodentate nitrate species (1290 cm^{-1}) were sharply elevated in the intensity of absorption.

Fig. 10 showed the DRIFT spectra of NH_3 adsorption for 30 min and purged by He for 30 min on various CaMnTi catalysts under 150 °C. Several bands in the range of 900–1700 cm^{-1} and 3100–3400 cm^{-1} were detected. According to the literature [61], the bands at 965 and 931 cm^{-1} could be assigned to the weakly

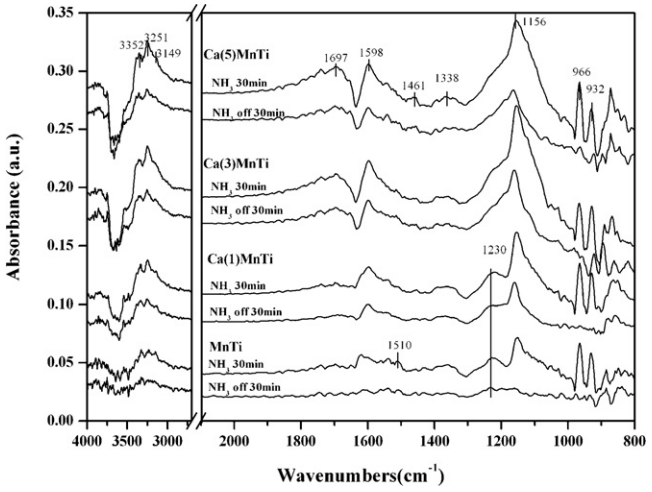

Fig. 10. DRIFT spectra taken at 150 °C upon passing 1000 ppm NH_3/He and evacuation over various CaMnTi catalysts for 30 min.

adsorbed NH_3 or gas phase NH_3, which were easily removed by the evacuation. The bands at 1598 and 1230, 1156 cm^{-1} were assigned to asymmetric and symmetric bending vibrations of the N—H bonds in NH_3 coordinately linked to Lewis acid sites [28,62,63], while the bands at 1461 cm^{-1} and in the range of 1850–1640 cm^{-1} were attributed to asymmetric and symmetric bending vibrations of NH_4^+ species on Brönsted acid sites [63]. In the NH stretching region, bands were found at 3352, 3251, and 3149 cm^{-1}. Some negative bands around 3700 cm^{-1} were also detected, which originated from the surface O-H stretching [62]. As the NH_3 adsorbed on the MnTi catalyst for 30 min, the weak band at 1510 cm^{-1} was detected, which was ascribed to the scissoring mode of an amide species (—NH_2) [62], formed by hydrogen abstraction from coordinated ammonia. Meanwhile, the band of 1338 cm^{-1} was due to the wagging mode of amide species (—NH_2). It is unsurprising that intensity of these NH_3 adsorption induced bands would increase after Ca doping since great enhancement in the surface area (see NH_3-TPD result). However, the Brönsted acid sites, which was identified by the enhanced intensity of symmetric bend vibration of NH_4^+ (approximately 1697 cm^{-1}), appeared and ascended successively with the rising of Ca doping content, which maybe attributed to the increase in surface hydroxyl concentration after Ca doping [63].

4. Discussions about the DRIFT results

In the study of NO adsorption DRIFT, it was found that the Ca doping would lead to an appearance of NO^- species during the adsorption process and an increase of NO_2^- species on the surface. It had been reported by Cerruti et al. [59] that when NO was adsorbed on the MgO surface, the gaseous NO would react with superficial O^{2-} which was a Lewis basic site to form adsorbed NO^- and NO_2^- species. As such, a similar reaction would take place on the Ca doped catalyst that two NO molecules would obtain an electron, respectively, to form NO^- and NO_2^- species around Ca sites, since Ca doping could improve the electron donation capacity of sample [17].

Subsequently, the NO^- species was readily oxidized and the concentration of the different nitrates drastically increased [64], especially the mondentate nitrate at 1290 cm^{-1}. It also could be proved in the DRIFT study of NO adsorption on Ca(5)MnTi catalyst (Fig. 9B) that there was a sharp improvement in the intensity of band at 1290 cm^{-1}. In the process of SCR reaction, the monodentate species M–O–NO_2 could rapidly react with the

neighboring adsorbed NH_4^+ or NH_3 to form more reactive intermediates M–O–$NO_2[NH_4^+]_2$ or M–O–$NO_2[NH_3]_2$, which would further react with gaseous NO to form N_2 and H_2O[65]. Meanwhile, the NO_2^- species was trended to bond with adsorbed NH_4^+ or NH_3 to form NH_4NO_2 species [66,67], which acted as an active intermediate in the process of SCR and would decompose readily to N_2 and H_2O. Moreover, the abundance of N_2O_4 and NO_2 species also implied that the oxidation of NO was greatly improved over Ca(5) MnTi catalyst, and the enhancement in monodentate nitrate and NO_2^- species induced by Ca doping facilitated the SCR reaction. Combined with the analysis of NO-TPD mentioned above, the comparison of the DRIFT spectra between these two samples confirmed that the Ca doping could improve the NO chemisorbed amount, which played an important role in NO reduction [55,68].

The NH_3 adsorption DRIFT spectra (Fig. 10) showed that the surface acid sites increased with the content of Ca, which was mainly due to the great increase in specific surface area, since the specific acidity would decrease after Ca doping. However, the Brönsted acid sites, which were almost not detected in MnTi sample, greatly increased after Ca doping. NH_4^+ species on Brönsted acid sites would quick react with NO_2^- and NO_2 at low temperature and form NH_4NO_2 [64,65] and NO_2 $[NH_4^+]_2$ [69], respectively, both of which were beneficial to fulfill the SCR process.

5. Conclusions

In this paper, a series of Ca modified CaMnTi catalysts were prepared by the sol–gel method, demonstrating better low-temperature SCR activity than MnTi catalyst. The main conclusions were drawn as follows:

1. Ca doping had strong promoting effect on catalytic activity of MnO_x/TiO_2. A NO conversion of over 90% could be obtained for Ca(5)MnTi sample at 140 °C, which were more than two time of that for undoped sample.
2. Based on the characterizations by BET, XRD, TEM, TPR and XPS, it was concluded that manganese oxides were better dispersed in the catalysts after Ca doping. Calcium would interact with manganese oxides and titania to form solid solution phase. Therefore, the better dispersion of Mn and Ti, the higher surface area and pore volume.
3. By means of NO-TPD and DRIFT experiments, it was found that the NO chemisorption and oxidation could be enhanced by Ca doping, especially, the surface monodentate nitrate and NO_2^- species was greatly increased, This change would promote the activity since these ad-NO_x species was an important SCR reaction intermediate at low temperature. XPS results also confirmed this finding by the increase in the chemisorbed oxygen content.
4. NH_3-TPD results showed that Ca doping would have negative effect on the specific acidity. However, it was found that Brönsted acid sites, was greatly improved by the introduction of Ca, which was mainly due to the increase in surface hydroxyl concentration after Ca doping.

Acknowledgments

The work is financially supported by the National Natural Science Foundation of China (No. 50908201), Natural Science Foundation of Zhejiang Province (Y5090053), Changjiang Scholar Incentive Program, Open Foundation of Zhejiang Provincial Environmental Pollution Control Technique Key Lab and Fundamental Research Funds for the Central Universities.

Appendix A. Supplementary data

Supplementary data associated with this article can be found, in the online version, at http://dx.doi.org/10.1016/j.apcatb.2012.09.003.

References

[1] G. Busca, L. Lietti, G. Ramis, F. Berti, Applied Catalysis B: Environmental 18 (1998) 1–36.
[2] G. Busca, M.A. Larrubia, L. Arrighi, G. Ramis, Catalysis Today 107 (2005) 139–148.
[3] T.S. Park, S.K. Jeong, S.H. Hong, S.C. Hong, Industrial and Engineering Chemistry Research 40 (2001) 4491–4495.
[4] F. Kapteijn, L. Singoredjo, A. Andreini, J.A. Moulijn, Applied Catalysis B: Environmental 3 (1994) 173–189.
[5] L. Singoredjo, R. Korver, F. Kapteijn, J. Moulijn, Applied Catalysis B: Environmental 1 (1992) 297–316.
[6] P.R. Ettireddy, N. Ettireddy, S. Mamedov, P. Boolchand, P.G. Smirniotis, Applied Catalysis B: Environmental 76 (2007) 123–134.
[7] Z.B. Wu, B.Q. Jiang, Y. Liu, W.R. Zhao, B.H. Guan, Journal of Hazardous Materials 145 (2007) 488–494.
[8] M. Richter, A. Trunschke, U. Bentrup, K.W. Brzezinka, E. Schreier, M. Schneider, M.M. Pohl, R. Fricke, Journal of Catalysis 206 (2002) 98–113.
[9] M. Stanciulescu, G. Caravaggio, A. Dobri, J. Moir, R. Burich, J.-P. Charland, P. Bulsink, Applied Catalysis B: Environmental 123–124 (2012) 229–240.
[10] G. Qi, R.T. Yang, Journal of Catalysis 217 (2003) 434–441.
[11] F. Eigenmann, M. Maciejewski, A. Baiker, Applied Catalysis B: Environmental 62 (2006) 311–318.
[12] G. Marbán, T. Valdés-Solís, A.B. Fuertes, Journal of Catalysis 226 (2004) 138–155.
[13] G. Qi, R.T. Yang, Applied Catalysis B: Environmental 44 (2003) 217–225.
[14] Z.B. Wu, R.B. Jin, Y. Liu, H.Q. Wang, Catalysis Communications 9 (2008) 2217–2220.
[15] M.A. Zamudio, N. Russo, D. Fino, Industrial and Engineering Chemistry Research 50 (2011) 6668–6672.
[16] H. Song, U.S. Ozkan, Journal of Physical Chemistry A 114 (2010) 3796–3801.
[17] L. Xue, H. He, C. Liu, C.B. Zhang, B. Zhang, Environmental Science and Technology 43 (2009) 890–895.
[18] D. Yang, J.H. Li, M.F. Wen, C.L. Song, Catalysis Today 139 (2008) 2–7.
[19] L. Chen, J.H. Li, M.F. Ge, Chemical Engineering Journal 170 (2011) 531–537.
[20] F.S. Tang, B.L. Xu, H.H. Shi, J.H. Qiu, Y. Fan, Applied Catalysis B: Environmental 94 (2010) 71–76.
[21] Y. Liu, T.T. Gu, Y. Wang, X.L. Weng, Z.B. Wu, Catalysis Communications 18 (2012) 106–109.
[22] S. Vargas, R. Arroyo, E. Haro, R. Rodríguez, Journal of Materials Research 10 (1999) 3932–3935.
[23] P. Forzatti, Catalysis Today 62 (2000) 51–65.
[24] L. Lietti, J. Svachula, P. Forzatti, G. Busca, G. Ramis, P. Bregani, Catalysis Today 17 (1993) 131–140.
[25] P.G. Smirniotis, P.M. Sreekanth, D.A. Peña, R.G. Jenkins, Industrial and Engineering Chemistry Research 45 (2006) 6436–6443.
[26] C.K. Luo, J.H. Li, Y.Q. Zhu, J.M. Hao, Catalysis Today 119 (2007) 48–51.
[27] L. Chmielarz, P. Kuśtrowski, M. Zbroja, B. Gil-Knap, J. Datka, R. Dziembaj, Applied Catalysis B: Environmental 53 (2004) 47–61.
[28] W.S. Kijlstra, D.S. Brands, E.K. Poels, A. Bliek, Journal of Catalysis 171 (1997) 208–218.
[29] A.N. Pour, S.M.K. Shahri, H.R. Bozorgzadeh, Y. Zamani, A. Tavasoli, M.A. Marvast, Applied Catalysis A: General 348 (2008) 201–208.
[30] S. Guerrero, I. Guzmán, G. Aguila, B. Chornik, P. Araya, Applied Catalysis B: Environmental 123–124 (2012) 282–295.
[31] J. Carnö, M. Ferrandon, E. Björnborn, S. Järås, Applied Catalysis A: General 155 (1997) 265–281.
[32] F.D. Liu, H. He, Y. Ding, C.B. Zhang, Applied Catalysis B: Environmental 93 (2009) 194–204.
[33] E.P. Reddy, B. Sun, P.G. Smirniotis, Journal of Physical Chemistry B 108 (2004) 17198–17205.
[34] Z.B. Wu, B.Q. Jiang, Y. Liu, Applied Catalysis B: Environmental 79 (2008) 347–355.
[35] X.F. Tang, J.H. Li, L. Sun, J.M. Hao, Applied Catalysis B: Environmental 99 (2010) 156–162.
[36] J.E. Moulder, W.F. Stickle, P.E. Sobol, K.D. Bomben, Handbook of X-ray Photoelectron Spectroscopy, Physical Electronics Inc., Minnesota, USA, 1995, pp. 68–69.
[37] M.S.P. Francisco, V.R. Mastelaro, Journal of Physical Chemistry B 105 (2001) 10515–10522.
[38] T. Kasuga, M.M. Hiramatsu, A. Hoson, T. Sekino, K. Niihara, Advanced Materials 11 (1999) 1307–1311.
[39] J.J. Yang, Z.S. Jin, X.D. Wang, W. Li, J.W. Zhang, S.L. Zhang, X.Y. Guo, Z.J. Zhang, Dalton Transactions (2003) 3898–3901.
[40] M.A. Khan, H.T. Jung, O.B. Yang, Journal of Physical Chemistry B 110 (2006) 6626–6630.
[41] X. Zhang, L.Y. Ji, S.C. Zhang, W.S. Yang, Journal of Power Sources 173 (2007) 1017–1023.

[42] M. Chigane, M. Ishikawa, Journal of the Electrochemical Society 147 (2000) 2246–2251.
[43] D.A. Peña, B.S. Uphade, P.G. Smirniotis, Journal of Catalysis 221 (2004) 421–431.
[44] N. Ohtsu, K. Sato, K. Saito, K. Asami, T. Hanawa, Journal of Materials Science: Materials in Medicine 18 (2007) 1009–1016.
[45] T. Hanawa, S. Hiromoto, K. Asami, Applied Surface Science 183 (2001) 68–75.
[46] M. Kang, E.D. Park, J.M. Kim, J.E. Yie, Applied Catalysis A: General 327 (2007) 261–269.
[47] M. Schindler, F.C. Hawthorne, M.S. Freund, P.C. Burns, Geochimica et Cosmochimica Acta 73 (2009) 2488–2509.
[48] L. Chen, J.H. Li, M.F. Ge, R.H. Zhu, Catalysis Today 153 (2010) 77–83.
[49] M. Kantcheva, Journal of Catalysis 204 (2001) 479–494.
[50] N. Tang, Y. Liu, H.Q. Wang, Z.B. Wu, Journal of Physical Chemistry C 115 (2011) 8214–8220.
[51] M. Machida, M. Uto, D. Kurogi, T. Kijima, Chemistry of Materials 12 (2000) 3158–3164.
[52] M. Machida, D. Kurogi, T. Kijima, Chemistry of Materials 12 (2000) 3165–3170.
[53] K. Hadjiivanov, V. Bushev, M. Kantcheva, D. Klissurski, Langmuir 10 (1994) 464–471.
[54] Y.H. Yeom, B. Wen, W.M.H. Sachtler, E. Weitz, Journal of Physical Chemistry B 108 (2004) 5386–5404.
[55] R.B. Jin, Y. Liu, Z.B. Wu, H.Q. Wang, T.T. Gu, Chemosphere 78 (2010) 1160–1166.
[56] M. Casapu, O. Kröcher, M. Mehring, M. Nachtegaal, C. Borca, M. Harfouche, D. Grolimund, Journal of Physical Chemistry C 114 (2010) 9791–9801.
[57] N. Apostolescu, T. Schroder, S. Kureti, Applied Catalysis B: Environmental 51 (2004) 43–50.
[58] K. Hadjiivanov, Catalysis Reviews – Science and Engineering 42 (2000) 71–144.
[59] L. Cerruti, E. Modone, E. Guglielminotti, E. Borello, Journal of the Chemical Society, Faraday Transactions 1 70 (1974) 729–739.
[60] M.J.D. Low, R.T. Yang, Journal of Catalysis 34 (1974) 479–489.
[61] G. Qi, R.T. Yang, R. Chang, Applied Catalysis B: Environmental 51 (2004) 93–106.
[62] L. Chen, J.H. Li, M.F. Ge, Environmental Science and Technology 44 (2010) 9590–9596.
[63] M.A. Larrubia, G. Ramis, G. Busca, Applied Catalysis B: Environmental 27 (2000) 145–151.
[64] K. Hadjiivanov, H.K. Zinger, Physical Chemistry Chemical Physics 2 (2000) 2803–2806.
[65] H. Chen, A. Sayari, A. Adnot, F. Larachi, Applied Catalysis B: Environmental 32 (2001) 195–204.
[66] Q. Sun, Z.X. Gao, B. Wen, W.M.H. Sachtler, Catalysis Letters 78 (2002) 1–5.
[67] A. Grossale, I. Nova, E. Tronconi, D. Chatterjee, M. Weibel, Topics in Catalysis 52 (2009) 1837–1841.
[68] T. Tanaka, T. Okuhara, M. Misono, Applied Catalysis B: Environmental 4 (1994) 1–9.
[69] R.Q. Long, R.T. Yang, Journal of Catalysis 207 (2002) 224–231.